Identifying Anomalous Regions of Vegetation Change From 2000 to 2020, China: Driving Forces, Probability, and Colocation Patterns

Xinyue Zhang, Li Peng, Jing Tan, Huijuan Zhang, and Huan Yu

***Abstract*—Differentiating between the effects of climate change and human activities on vegetation change is important in the context of vegetation restoration and management. In this study, we used the Theil–Sen slope and Mann–Kendall test to analyze the spatiotemporal changes in vegetation cover in China from 2000 to 2020, defining a series of anomalous regions. The probability of vegetation greening and browning under different climates and population pressures was evaluated using copula functions, and their spatial aggregation was studied through the colocation quotient. Geodetector was then used to analyze the influencing factors of vegetation change in these anomalous regions. Our findings have shown that the vegetation recovery rate in northern China has surpassed that of southern China. Precipitation and temperature across the entire region showed a positive feedback relationship with normalized difference vegetation index, indicating substantial spatial heterogeneity. Anomalous regions of vegetation change were predominantly concentrated in eastern China. The statistical probability of the copula function reflects that the synchronization probability of vegetation response to the external environment is higher. The sensitivity of temperature to vegetation is higher than that of precipitation and higher than that of population density. However, in the Tibetan Plateau and western arid zone, the feedback of population density has exceeded that of precipitation due to improvements in land management from population concentration. The findings have also shown that the vegetation dynamics are primarily influenced by soil water content, with the slope aspect having a minimal influence. Nonlinear interactions were observed among most of the influencing factors, with the interaction between soil water content and altitude being the strongest.**

***Index Terms*—Anomalous region, climate change, colocation patterns, human activity, normalized difference vegetation index (NDVI).**

I. Introduction

As a key component of terrestrial ecosystems, vegetation plays a pivotal role in connecting various spheres, such as the atmosphere, hydrosphere, and soil. It is a means of soil and water conservation while also regulating carbon balance within ecosystems [1], [2], [3]. Vegetation is a key indicator of climate change, with heightened sensitivity at high latitudes and altitudes [4]. The normalized difference vegetation index (NDVI) is an indicator that describes the growth status of vegetation, and biomass [5], [6]. It is broadly applied in the study of vegetation dynamics at various spatial scales [7], [8]. NDVI has been used to identify the responses of vegetation to climate change and assess changes in ecological environment quality [9], [10]. Due to the vast expanse of China and the complexity of its climate dynamics and human activities, current macroresearch on China's vegetation cover mainly focuses on the classification of areas of vegetation cover increase and degradation and the correlation with climate [11], [12], [13]. However, to date, there has been relatively little research on potentially anomalous regions that contrast with the conventional patterns of vegetation responses to climate change and human intervention. Anomalous regions are areas where vegetation changes deviate from the anticipated outcomes of climate change and human influence.

Previous studies have shown that changes in vegetation cover are mainly due to the combined effects of climate and human activities [14], [15], [16]. Browning of vegetation cover by human activities such as urban expansion, destructive deforestation, and poor land use, deepens the fragmentation of regional landscapes and thus weakens the value of ecosystem services [17], [18]. Conversely, there are positive impacts from human interventions driving ecological restoration and conservation efforts to increase vegetation cover. China's Grain for Green and Natural Forest Protection Programs have successfully curbed desertification in the degraded karst regions of southwest China, thereby enhancing ecosystem resilience [19], [20], [21], [22]. As people have paid more attention to their health and well-being, the number of parks and green spaces in densely populated urban areas has increased [23], [24]. In China, significant fluctuations in land surface elevation and varying climates across regions contribute to a high spatial heterogeneity in vegetation distribution. Correlation analysis is often employed to assess these factors and understand their feedback effects [12], [25], [26]. An increase in temperature has led to an upward trend in the NDVI in certain high-latitude regions of the Northern Hemisphere [27]. Conversely, it has negatively affected vegetation growth in arid zones [13]. However, a contrasting scenario has unfolded in ecologically restored zones in the northwest [28].

Manuscript received 3 June 2024; revised 24 July 2024; accepted 6 August 2024. Date of publication 12 August 2024; date of current version 26 August 2024. This work was supported in part by the Sichuan and Technology Program under Grant 2022JDJQ0015, and in part by the Nation Key Research and Development Program of China under Grant 2022YFF1300701. *(Corresponding author: Li Peng.)*

Xinyue Zhang, Li Peng, Jing Tan, and Huijuan Zhang are with the College of Geography and Resources, Sichuan Normal University, Chengdu 610101, China, and also with the Key Laboratory of Land Resources Evaluation and Monitoring in Southwest, Ministry of Education, Sichuan Normal University, Chengdu 610066, China (e-mail: 20231101014@stu.sicnu.edu.cn; pengli@imde.ac.cn; 20221101032@stu.sicnu.edu.cn; 20231101026@stu.sicnu.edu.cn).

Huan Yu is with the College of Earth Science, Chengdu University of Technology, Chengdu 610059, China (e-mail: yuhuan10@cdut.edu.cn).

Digital Object Identifier 10.1109/JSTARS.2024.3441765

© 2024 The Authors. This work is licensed under a Creative Commons Attribution-NonCommercial-NoDerivatives 4.0 License. For more information, see https://creativecommons.org/licenses/by-nc-nd/4.0/

Meanwhile, in selected areas of the Tibetan Plateau, an increase in precipitation does not always lead to vegetation greening [29]. Instead, it may trigger a negative NDVI shift by attenuating solar radiation and temperature [30]. Therefore, when studying vegetation responses to the environment, it is crucial to examine it according to the geographic area according to specific research objectives.

In the past few decades, China's terrestrial vegetation ecosystem has improved, but the vegetation recovery in some regions is different from other regions due to the rapid change of climate and the impact of human activities [31], [32]. Although traditional NDVI studies mostly capture temporal and spatial changes in district vegetation cover [33], [34], it is important to recognize that alterations in vegetation cover are representations, often failing to reveal hidden information within a region. Therefore, it is of practical significance to identify and attribute anomalous regions. Areas with increased human activities but green vegetation, such as areas with decreased precipitation but significantly improved vegetation, can be called anomalous regions. Identifying and understanding these anomalous regions has considerable importance for policy-making related to ecological restoration and land management practices. In examining vegetation responses to climate change and human impacts, prior studies have predominantly concentrated on variations in NDVI, neglecting trends in the average annual NDVI. Here, we define this as vegetation change and make it the focal point of our research.

NDVI data spanning 2000–2020 were used to classify vegetation dynamics across China, and a series of anomalous regions were defined in this research. A copula conditional probability model was used to study the potential of vegetation cover scenarios under different states. The probabilistic relationship between temperature and precipitation trends, population change, and degree of vegetation cover was analyzed. Through correlation analysis and the colocation quotient (CLQ), we examined the statistical and spatial interactions among various anomalous regions, climatic factors, and socioeconomic variables. Furthermore, we aimed to determine the factors influencing spatial correlations and changes in the NDVI. The method used is illustrated in Fig. 1.

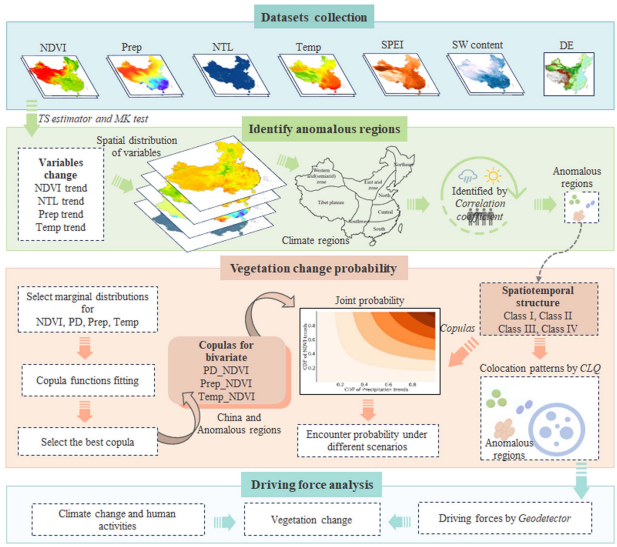

Fig. 1. Technical flowchart.

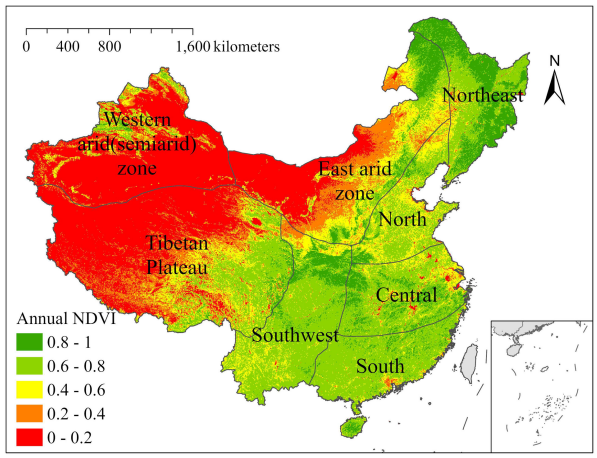

Fig. 2. Average annual NDVI from 2000 to 2020 and the China climate zone division.

II. Materials and Methods

A. Data Sources

Owing to the substantial area of inland China, different climatic conditions in various regions have shown considerable variations in their impact on NDVI. To more effectively investigate the influence of rates of climate change on NDVI variations on distinct zones, according to the zoning criteria proposed by Zhang and Xiao [35], [36], we divided the inland region into eight climatic zones for research, that is, the central, eastern arid zone, north, northeast, south, southwest, Tibetan Plateau, and western arid (semiarid) zone (Fig. 2).

The NDVI datasets were obtained from the MOD13Q1 NDVI monthly datasets processed by Gao [37], with a spatial resolution of 250 m. From 2000 to 2020, we used the maximal component approach to extract the annual NDVI. Given that datasets may contain negative NDVI values primarily because of topographical factors, it is crucial to eliminate the impact of such raster data during the data analysis. Data projection was aligned with the research objectives for accurate analysis.

Nighttime light data (NTL) were obtained from annually published datasets on the Harvard Dataverse, with a spatial resolution of 500 m [38]. Temperature and precipitation data for the same timeframe were amalgamated from monthly data with a resolution of 1 km [39]. Population density (PD) data for 2000 and 2020 include 1 km spatial resolution data available on the WorldPop (https://www.worldpop.org/). To evaluate the driving forces behind NDVI fluctuations, we integrated 1 km spatial resolution data for the Standardized Precipitation Evapotranspiration Index (SPEI), soil water (SW) content, and a 90 m spatial resolution Digital Elevation Model sourced from Peng and Zheng [40], [41]. For more thorough data analysis, all the datasets were resampled to a spatial resolution of 5 km and standardized according to the same spatial reference.

B. Theil–Sen (TS), Median Slope, and Mann–Kendall (MK) Tests

The TS slope is often used in trend analysis, characterized by its independence from data distribution assumptions [42], [43]. By integrating the TS slope with the MK test, we computed and evaluated the trends in NDVI from 2000 to 2020.

$$\beta = Median\left(\frac{v_j - v_i}{j - i}\right), \forall j > i. \tag{1}$$

Equation (1) displays the formula of slope. β is the calculated slope of the data change, the median is the solution of the median of the data, and v_j and v_i are the time-series data. In the time series, a rising trend is shown by a positive β value, while a downward trend is indicated by a negative β value. The MK test plays a critical role in assessing the significance of time-series data. Z denotes the standardized statistical test and n signifies the total statistical quantity of time-series data, as defined in the following equations:

$$Z = \begin{cases} \frac{S-1}{\sqrt{\mathrm{var(s)}}}, & S > 0 \\ 0, S = 0, \\ \frac{S+1}{\sqrt{\mathrm{var(s)}}}, S < 0 \end{cases} \tag{2}$$

$$S = \sum_{i=1}^{n-1} \sum_{j=i+1}^{n} \mathrm{sgn}\left(a_j - a_i\right) . \tag{3}$$

In (3) a_i and a_j are the average NDVI of years i and j. The null hypothesis is rejected when $|Z| > Z_{1\text{-}\alpha/2}$, which suggests a substantial trend in the NDVI time series at the confidence level α. $|Z|$ exceeding 1.96 indicates passing the significance test at a 95% confidence level.

C. Copula-Based Assessment Approach

The copula function is frequently employed in constructing correlation models for multidimensional random variables [44]. As this method does not require variables to follow the same distribution type, it has been widely used in hydrological research [45], [46]. The adaptability of Copula functions enables them to accommodate diverse marginal distributions and dependency structures, crucial for analyzing ecological data characterized by significant heterogeneity. Selecting an appropriate copula type enhances data fitting and boosts the model's predictive capabilities. This study employs Copula functions to assess the concurrent probability of NDVI change rates in relation to variations in precipitation, temperature, and PD dynamics.

The main objective of this research is to employ copula functions to calculate the joint probabilities of NDVI dynamics for changes in temperature (Temp_NDVI), precipitation (Prep_NDVI), and PD (PD_NDVI). Maximum likelihood estimation was used to calculate the parameters of five copula functions including t copula, Frank copula, Clayton copula, Gaussian copula, and Gumbel copula. The Euclidean distance between the copula function and the empirical copula function was computed, and the copula function with the minimum Euclidean distance was chosen as the optimal one.

D. CLQ

Introduced by Leslie and Kronenfeld [47], the global colocation quotient (GCLQ) evaluates the overall colocation patterns between two types of point objects. However, challenges arise when factors like population and land use impede its efficacy in assessing internal colocation patterns in a specific region. To address this, Cromley et al. [48] devised a local colocation quotient (LCLQ) derived from the GCLQ, producing maps that offer enhanced insights into the spatial relationships between elements.

$$GCLQ_{A_i \to B} = \frac{\mathrm{N_{A\to B}}/\mathrm{N_A}}{N_B\,(N-1)}. \tag{4}$$

In (4), $\mathrm{GCLQ_{A\to B}}$ denotes the extent to which Type A points are attracted by Type B points. The N, $\mathrm{N_A}$, and $\mathrm{N_B}$ represent the total number of research samples, type A points, and type B points, respectively, in the study region. The number of Type A points that are closest to Type B points is represented by the symbol $\mathrm{N_{A\to B}}$.

The observed percentage of Type B points that are closest neighbors of Type A points is reflected in the numerator. In the meantime, the denominator is the percentage of Type B points that are closest neighbors of Type A points in a random scenario. If $\mathrm{GCLQ_{A\to B}}$ exceeds 1, it indicates that $\mathrm{A_i}$ is closest to the Type B point. A larger value indicates a stronger association between the types. Conversely, if $\mathrm{GCLQ_{A\to B}}$ is less than 1, it suggests that the types tend to be dispersed.

$$LCLQ_{A_i \to B} = \frac{\mathrm{N_{A_i\to B}}}{N_B\,(N-1)}. \tag{5}$$

In (5), the geographically weighted average of the closest Type B points within the designated bandwidth of Type A points is represented by $\mathrm{N_{Ai\to B}}$, while $\mathrm{LCLQ_{Ai\to B}}$ describes the degree to which Type B points are attached to the $\mathrm{A_i}$ point.

$$\mathrm{N}_{A_i \to \mathrm{B}} = \sum_{j=1(j\neq i)}^{N} \left(w_{ij} f_{ij} / \sum_{j=1(j\neq i)}^{N} w_{ij} \right) \tag{6}$$

$$w_{ij} = exp\left(-0.5 * \frac{d_{ij}^2}{d_{ib}^2}\right). \tag{7}$$

In (6), A_i stands for the ith type A point, and f_{ij} denotes if j is a Type B point (1 means yes, otherwise 0). Here, w_{ij} stands for point the weight of point j, signifying the importance of j for the ith A-type point. d_{ij} represents the distance between the ith point of Type A and point j, whereas d_{ib} represents the bandwidth surrounding the ith type A point. Each neighborhood of A_i in (7) was given a geographical weight value using a Gaussian kernel density function. This function ensures that points closer to Point A receive higher weights, reflecting their greater importance. A 999-time Monte Carlo simulation was used to confirm the results and determine the significance of the LCLQ results.

E. Geodetector

The Geodetector statistical method [49], was used to identify spatial heterogeneity and determine the underlying driving

TABLE I
VARIABLE GEODETECTOR SELECTION

Variable	Description
Explained variable	Variable
NDVI_trend	Trends in NDVI from 2000 to 2020
Explanatory variable	
NTL_trend	Trends in NTL from 2000 to 2020
Temp_trend	Trends in temperature from 2000 to 2020
Prep_trend	Trends in precipitation from 2000 to 2020
SW_trend	Trends in SW content from 2000 to 2020
SPEI_trend	Trends in SPEI from 2000 to 2020
Elevation	The average elevation in a pixel
Gradient	The average gradient in a pixel
Aspect	Average aspect in a pixel

forces influencing trends in NDVI changes. The utilization of this method aimed to evaluate the explanatory power and interactions among the factors influencing vegetation dynamics. The independent variables (X) and dependent variables (*Y*) influencing vegetation change are outlined in Table I. It has been demonstrated that population density and GDP data can be derived from NTL data. While population density can provide insights into human activity levels, it may not comprehensively capture local economic development. The NTL data and human economic activities have an association [50], [51] which leads to the use of NTL data as a representation of human activities.

Among the factors considered, aspect, gradient, and elevation showed significant interannual variations, leading to their inclusion as driving factors in the analysis. This study has focused on determining how these factors have contributed to the observed changes in NDVI over the study period.

1) Factor Detector: This method shows that the stronger the spatial resemblance between the independent variable *X* and the dependent variable *Y*, the greater the impact. This relationship was quantified using the statistical measure q.

$$q = 1 - \frac{\sum_{h=1}^{L} N_h \partial_h^2}{N \partial^2}. \tag{8}$$

In (8), where $h = 1 \ldots L$ represents the strata of variable *Y* or factor *X*. N_h and N represent the number of units in stratum h and in the entire area, respectively. ∂_h^2 and ∂^2 denote the variance of *Y* values in stratum h and the entire area, respectively. With values spanning 0–1, parameter q represents the explanatory power of each influencing factor on the trend of NDVI. A larger q value implies a more substantial and influential impact of the corresponding factor on changes in the independent variable.

2) Interaction Detector: It is mostly used to examine the relationship between two variables and add up the q values to find out if there is a rise or fall in the explanatory power of the two factors. Definitions reference Table II.

TABLE II
TYPES OF INTERACTION BETWEEN THE TWO FACTORS AS DEFINED IN GEODETECTOR

Interaction	Description
Weakened, nonlinear	$q(X_1 \cap X_2) < Min\,(q(X_1), q(X_2))$
Weakened, single factor nonlinear	$Min(q(X_1), q(X_2)) < q(X_1 \cap X_2) < Max(q(X_1), q(X_2))$
Enhance, double factors	$q(X_1 \cap X_2) > Max(q(X_1), q(X_2))$
Independent	$q(X_1 \cap X_2) = q(X_1) + q(X_2)$
Enhance, nonlinear	$q(X_1 \cap X_2) > q(X_1) + q(X_2)$

III. RESULTS

A. Factor Characteristic Analysis

Fig. 2 shows the spatial heterogeneity of the average annual NDVI in China from 2000 to 2020. The trend shows a decline in annual NDVI from the southeast coastal terrains toward the northwest inland expanses. In the eastern monsoon regions with favorable hydrothermal conditions, woodlands have dominated, leading to a higher annual NDVI. In contrast, the arid climate of the northwestern regions, which is characterized by deserts and barren lands, has led to a lower average annual NDVI. The annual NDVI shows a fluctuating upward trend at a rate of 0.00233 per year, reflecting the gradual increase in the average annual temperature at 0.0158°C/year and precipitation at 2.47 mm/year.

By using the TS slope and MK test on the NDVI, temperature, precipitation, NTL data, SPEI, and SW content, Fig. 3 illustrates the spatial distribution of the shifting trends. Refining the portrayal of PD changes with the adjusted 2000 and 2020 census data, as shown in Fig. 3(h), provides insights into the PD dynamics. During the previous 20 years, China has undergone rapid economic growth, with PD changes primarily concentrated in the eastern coastal areas and key urban agglomerations. The NTL data reflects the level of human activity, and changes in space are in line with PD shifts. A total of 81.06% of the region has shown an increase in temperature and 28.44% has had a decrease in precipitation.

Based on the TS slope analysis and outcomes of the MK test, the variations in NDVI were categorized into three levels under the 95% significance test criterion. These were significant increases, insignificant changes, and significant decreases, as shown in Fig. 4. Analysis of the NDVI pixel counts across different change categories and regions showed that 46.52% of China exhibited significant vegetation improvement, 50.77% remained unchanged, and 2.71% experienced significant degradation. Regions such as the eastern arid zone, north, and northeast showed significant NDVI improvements, exceeding 50% of the region. Conversely, areas with significant decreases were predominantly concentrated in the upper Pearl River Delta, Yangtze River Economic Belt, and Yangtze River Delta. Some vegetation degradation was also observed in the Ili River Valley, the northwestern part of the eastern arid zone, the Tibetan Plateau, and the southern portion of the southwest. These areas and the distribution of towns and urban centers are highly connected.

B. Partitioning of Anomalous Regions

To investigate the anomalous regions in the NDVI change trends, a pixel-by-pixel correlation analysis was conducted between the trends in temperature, precipitation, nighttime lights, and NDVI changes. The correlation and significance results are shown in Fig. 5. Temperature was positively correlated with NDVI in 62.61% of the region. It was primarily concentrated in southern China, the eastern and western sides of the East Arid

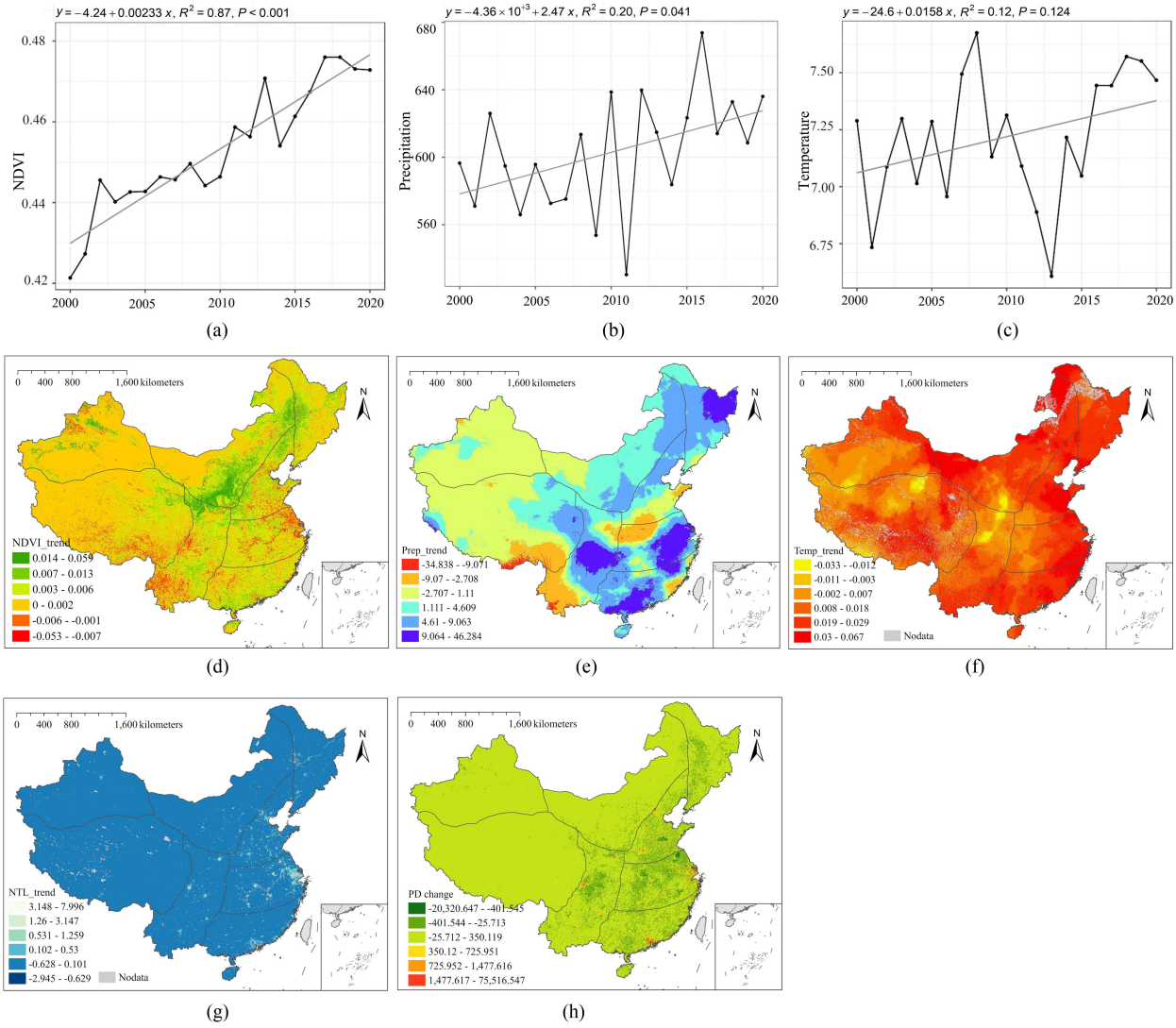

Fig. 3. Statistical charts and distribution of factors. (a)–(c) Signify interannual variations of NDVI, precipitation, and temperature, respectively. (d)–(g) Trends of NDVI, precipitation, temperature, and NTL from 2000 to 2020. (h) Evolution of population density from 2000 to 2020.

Zone, and the northern part of the Tibetan Plateau, with the latter two regions exhibiting higher correlation coefficients [Fig. 5(a)]. In contrast, 71.23% of the area had a positive correlation between precipitation and NDVI, predominantly in northern China, the northeastern part of the Tibetan Plateau, and some areas in the southwest [Fig. 5(b)].

The positive spatial relationship between NTL and NDVI correlation can be attributed to the diverse rates of change observed in NTL and NDVI during the analysis. A reduction in human activity also contributed to vegetation recovery. Scattered positive correlations between NTL data and NDVI were observed in Xinjiang. This was attributed to favorable water and heat conditions in the Ili River Valley, surrounding areas of the Tarim Basin, and lush oases. This has provided an environment conducive to vegetation growth that has made these areas more habitable and suitable for development [52].

With reference to the conclusions of some scholars, the criteria for anomaly region division are formulated and shown in Table III [13], [27], [53] [54]. Regions with anomalous vegetation change were classified into four types based on the criteria outlined in Table III. Within this framework, regions exhibiting a significant negative correlation between NDVI and temperature changes were categorized as Class I. Meanwhile, regions exhibiting a significant opposite relationship with precipitation were classified as Class II. Human activities associated

TABLE III
IDENTIFICATION CRITERIA FOR ANOMALOUS REGIONS

Variable	NDVI_ trend	Temperature_ NDVI	Precipitation_ NDVI	NTL_ NDVI
Class I	-	Negative*	-	-
Class II	-	-	Negative*	-
Class III	<0	-	-	Positive*
Class IV	>0	-	-	Positive*

* indicates passing the test at the 5% significance level.

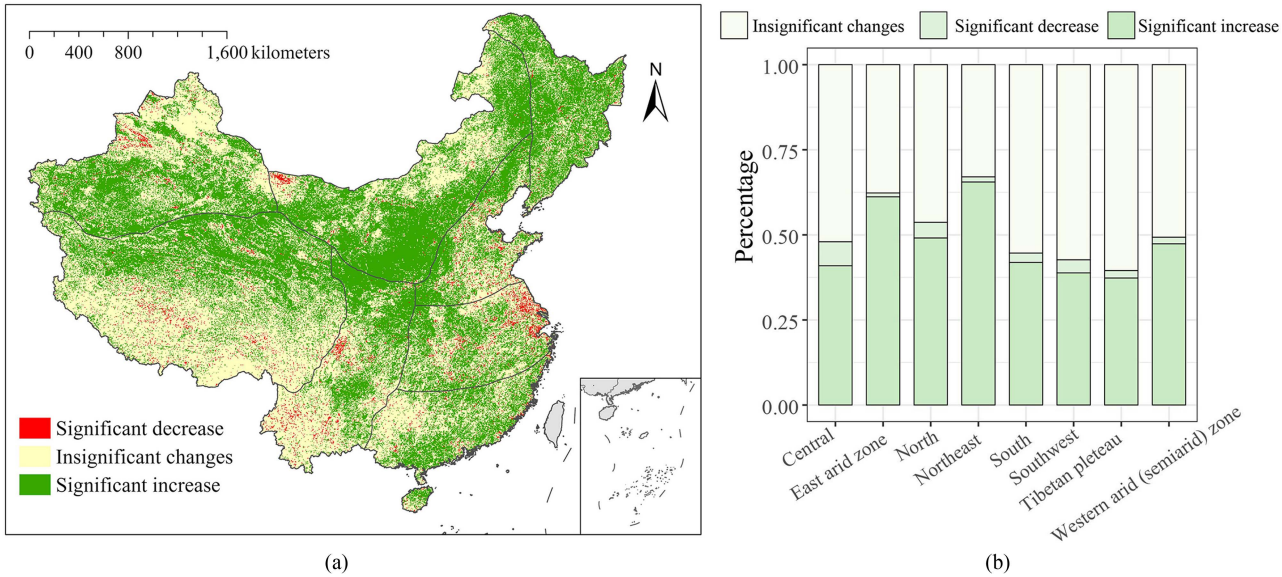

Fig. 4. Vegetation change distribution. (a) Spatial distribution of vegetation changes in various climatic zones. (b) Statistical map of vegetation change.

with urban development tend to negatively impact NDVI. Areas where the change in NTL was significantly positively correlated with the NDVI change were further subdivided into Class III and Class IV based on the NDVI change direction.

Traditional studies on NDVI changes may overlook local variations because the vegetation cover changes depicted are primarily representations. It is crucial to further examine the mechanisms underlying these representations and their driving forces. The spatial distributions of the four anomalous region classes are shown in Fig. 6(a). Class I was scattered throughout the spatial domain. Meanwhile, Class II had a horizontal distribution, mainly concentrated in the southern region of China. Class III, being the least abundant, was predominantly located in the central areas of economically developed regions. Meanwhile, Class IV was located in the Central Plains and southeastern coastal areas. The classifications of the anomalous regions are interconnected. Fig. 6(b) shows that Classes I and II have the largest number of intersections, primarily distributed in the eastern coastal cities of central China, northern regions of the Tibetan Plateau, and the Chengdu Plain region. The central region encompasses numerous cities with high urbanization levels. Despite increases in temperature and precipitation in some areas, the NDVI still indicates browning, which is primarily caused by human activity. Vegetation change does not respond solely to climate change.

C. Vegetation Change Conditional Probability Analysis

Various types of copula functions have distinct effects on the characterization of the dependence relationships between random variables. Five copula functions were used to model the marginal distribution function, and the most applicable copula function was chosen by comparing the minimum Euclidean distance. Among these, the Frank, t, and Gumbel copulas exhibited the highest frequency of occurrence. The joint distribution results between various variables and the change in NDVI are shown in Fig. 7.

To understand the conditional probabilities of vegetation increase and degradation under various external environmental changes such as temperature, precipitation, and PD, the cumulative distribution probabilities of variables with a value of zero were calculated for these four random variables. These values were the basis for the scenario delineation. External environmental variables are denoted as X, where a value greater than 0 indicates an increasing state. This reflects a positive trend in vegetation change, indicating favorable vegetation growth conditions, and an ameliorating phase for vegetation. Conversely, a value of less than 0 implies a decreasing state for X, signifying a negative trend in vegetation change and vegetation degradation.

Scenario A represents an increase in variable X, leading to vegetation improvement. Scenario B signifies a decrease in X, leading to vegetation greening. Scenario C indicates an increase in X, resulting in vegetation browning. Scenario D denotes a decrease in X, leading to vegetation browning. The probabilities of encountering vegetation changes under different scenarios were determined by applying statistical probability formulas, as outlined in Table IV. Climate demonstrated the highest sensitivity to vegetation, followed by precipitation, with PD ranking the lowest. The synchronous probability between PD and vegetation conditions exceeded that of precipitation in the Tibetan Plateau and western arid (semiarid) zone, highlighting a stronger positive correlation.

D. Colocation Patterns From Anomalous Regions

Using the CLQ spatial analysis tool, we examined the spatial correlation of the various anomalous regions. Because of the scattered distribution of anomalous regions and localized variations in precipitation, temperature, and NTL within specific geographic extents, setting excessively large bandwidths can

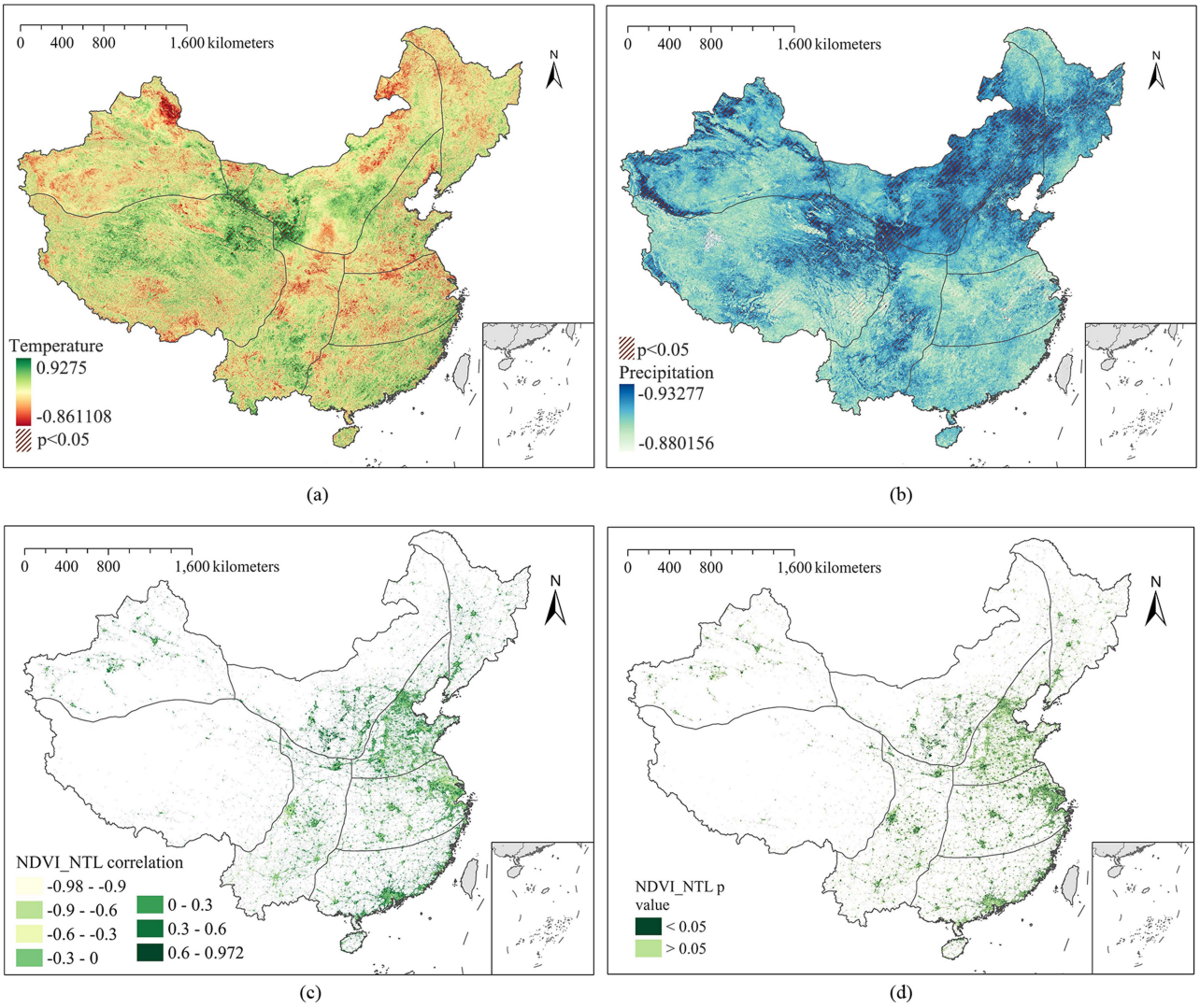

Fig. 5. Correlation and significance. (a) NDVI and temperature. (b) NDVI and precipitation. (c) and (d) Correlation and significance distributions of NDVI and NTL, respectively.

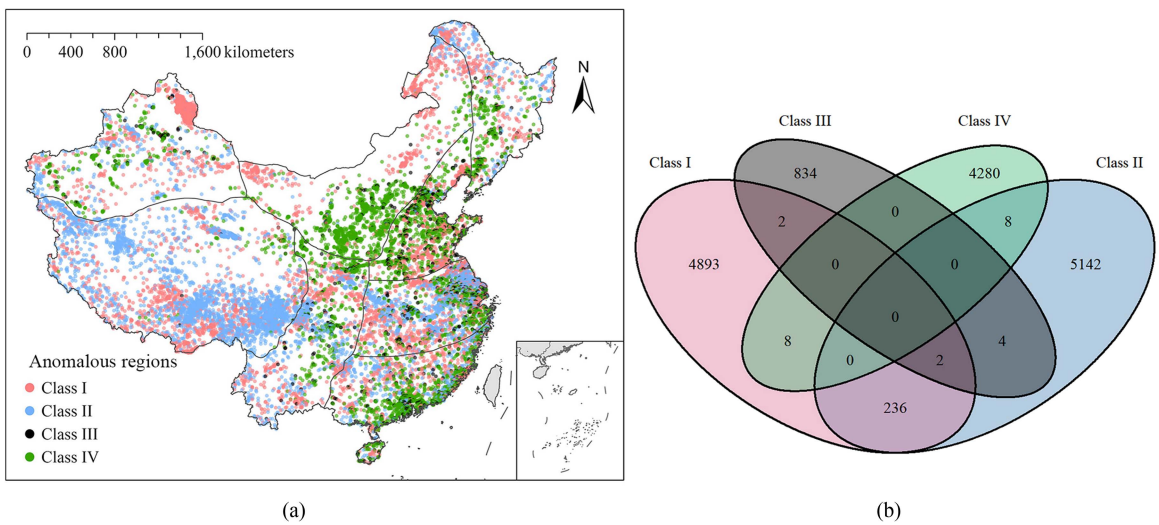

Fig. 6. (a) Distribution of anomalous regions. (b) Venn diagram of anomalous regions.

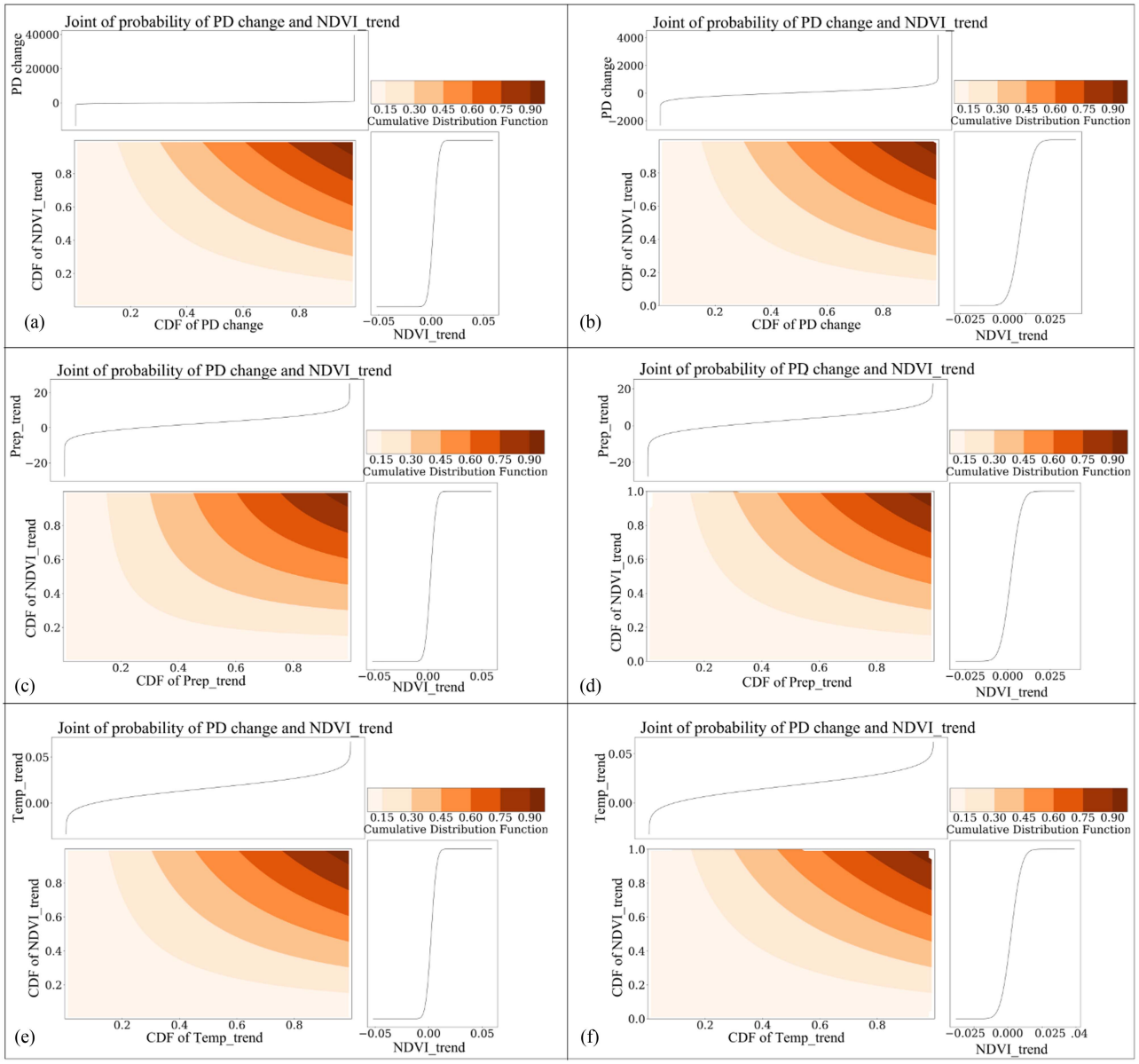

Fig. 7. Joint probability distribution between environmental variables and vegetation change. (a), (c), and (e) reflect China. (b), (d), and (f) reflect anomalous regions.

result in over-smoothed outcomes [55]. Through multiple experiments, distance bands of 10, 15, and 25 km were established. The GCLQ values between the four classes of anomalous regions consistently remained below 1. This indicated relative spatial independence among the distributions of anomalous regions. Table V shows that although the attraction strengths between different types of anomalous regions increase with bandwidth expansion, there was no significant colocation pattern across the entire region. This may be attributed to China's extensive land area and substantial internal geographical disparities at the overall scale.

Class II showed the highest attraction toward Class I, whereas Class II showed a significant affinity toward Class I. The mutual attraction between Class III and Class IV generally exceeded 0.9, suggesting a tendency toward mutual dependency between the NTL and NDVI anomalous regions. Class II exhibited the least attraction to Classes III and IV. However, although the GCLQ had an overall colocation pattern, it failed to capture localized variations in the strength of the associations. To address this limitation, the LCLQ was introduced to uncover the spatial variability of correlations between the two regions. In Fig. 8, the local colocation patterns between the different types are illustrated by using a bandwidth of 25 km. Given the absence of significant local colocation patterns between Class III and the other anomalous regions, Class III was excluded from the study.

The strong attraction of Class II toward Class I was mostly concentrated in the northern regions of the central region and southern Tibetan Plateau, as shown in Fig. 8(a). Overlaying the temperature and precipitation trends showed a decrease in rainfall in these anomalous regions of the Tibetan Plateau. This was accompanied by a slight decrease in temperature. However, vegetation has shown an increased sensitivity to temperature

TABLE IV
PROBABILITY OF ENCOUNTERING VEGETATION CHANGE UNDER DIFFERENT SCENARIOS

Scenario	China	Anomalous regions	Central	East arid zone	North	Northeast	South	Southwest	Tibetan Plateau	Western arid zone
					PD_NDVI					
A	0.4984	0.4331	0.2724	0.5125	0.4425	0.2954	0.3399	0.3593	0.6594	0.7121
B	0.3305	0.2821	0.4908	0.4193	0.4895	0.635	0.4924	0.4014	0.1413	0.1509
C	0.1027	0.1701	0.0957	0.0334	0.0337	0.03	0.0779	0.1269	0.1605	0.1026
D	0.0684	0.1147	0.1411	0.0348	0.0343	0.0396	0.0898	0.1124	0.0388	0.0344
					Prep_NDVI					
A	0.6715	0.5136	0.5905	0.9313	0.5727	0.909	0.7569	0.5434	0.533	0.5435
B	0.1692	0.2037	0.1728	0.0000	0.2451	0.0113	0.0715	0.2096	0.2654	0.3108
C	0.0943	0.1913	0.2004	0.0685	0.0979	0.078	0.1529	0.1277	0.1051	0.0728
D	0.065	0.0914	0.0363	0.0002	0.0843	0.0017	0.0187	0.1193	0.0965	0.0729
					Temp_NDVI					
A	0.7941	0.6723	0.7534	0.9065	0.8084	0.9284	0.8279	0.6716	0.7236	0.7924
B	0.0432	0.0428	0.0071	0.0217	0.0074	0.0000	0.0018	0.0783	0.0754	0.0595
C	0.1529	0.2695	0.2381	0.0718	0.1831	0.0716	0.1699	0.2359	0.1729	0.1372
D	0.0098	0.0154	0.0014	0.0000	0.0011	0.0000	0.0004	0.0142	0.0281	0.0109

TABLE V
GCLQ VALUES FOR VARIOUS TYPES OF ANOMALOUS REGIONS AT DIFFERENT BANDWIDTHS

Bandwidth	I			II			III			IV		
	10 km	15 km	25 km	10 km	15 km	25 km	10 km	15 km	25 km	10 km	15 km	25 km
I	-	-	-	0.4566	0.4601	0.4823	0.5838	0.5788	0.5945	0.3077	0.3219	0.3453
II	0.5009	0.4807	0.4878	-	-	-	0.4283	0.4212	0.4511	0.2066	0.2163	0.2323
III	0.5804	0.5908	0.6064	0.4157	0.4115	0.4327	-	-	-	0.9086	0.9143	0.9140
IV	0.3209	0.3302	0.3554	0.2250	0.2295	0.2434	0.9108	0.8916	0.9015	-	-	-

fluctuations. Rising temperatures lead to permafrost thawing, whereas reduced precipitation results in soil aridity and decreased vegetation cover [56].

The central area comprises several rapidly urbanizing developed cities, where extensive green spaces are being converted into urban areas. The expansion of these cities comes at the expense of significant green space loss, which primarily contributes to the decline in the NDVI. Class I shows a significant attraction to nighttime light anomalous regions, primarily concentrated in the developed coastal areas in the east. Temperature likely has a key role in driving surface NDVI changes in moist coastal plain areas in the east [57]. There was a significant degree of similarity in the colocation patterns of Class III with Class I [Fig. 8(b)] and Class IV [Fig. 8(c)] with Class I. Urbanization has had a detrimental impact on vegetation growth. Although urbanization can negatively affect vegetation growth, the establishment of numerous green parks within and around cities can lead to greening trends in certain areas. The warming effects of the urban heat island can also contribute to vegetation improvement [58].

Because of the nature of the LCLQ metrics that measure the attraction between Classes I and II, the degree of attraction between them is asymmetric. Regions with a strong attraction from Class I to Class II exhibited inconsistent spatial distributions. In the central region, there was a higher concentration of exceptional Class II, influenced by Class I [Fig. 8(d)] and impacted by urbanization. These anomalous regions have increased precipitation and temperatures, leading to vegetation degradation. Sparse anomalous regions also exist in Xinjiang, primarily because the vegetation in this region responds more sensitively to precipitation [59]. An increase in temperature alters the annual evaporation rate, leading to decreased humidity, which is detrimental to vegetation growth. Class III [Fig. 8(e)] and Class IV [Fig. 8(f)], which experience significant attraction from Class II, are predominantly located in southeastern coastal and inland economic centers. They have spatial distribution patterns similar to those illustrated in Fig. 8(b) and (c). These regions typically receive annual precipitation exceeding 1000 mm and show an increasing trend. However, vegetation within urban areas in these regions continues to be influenced by human activities.

Class VI and Class I [Fig. 8(g)] and Class VI and Class II [Fig. 8(h)] show significant separation in the southeastern coastal and Taihang Mountain areas. This has been driven by human interventions involving extensive land use changes and the performance of ecological conservation policies. This has shifted vegetation dynamics toward browning and greening, which no longer rely solely on natural climatic fluctuations.

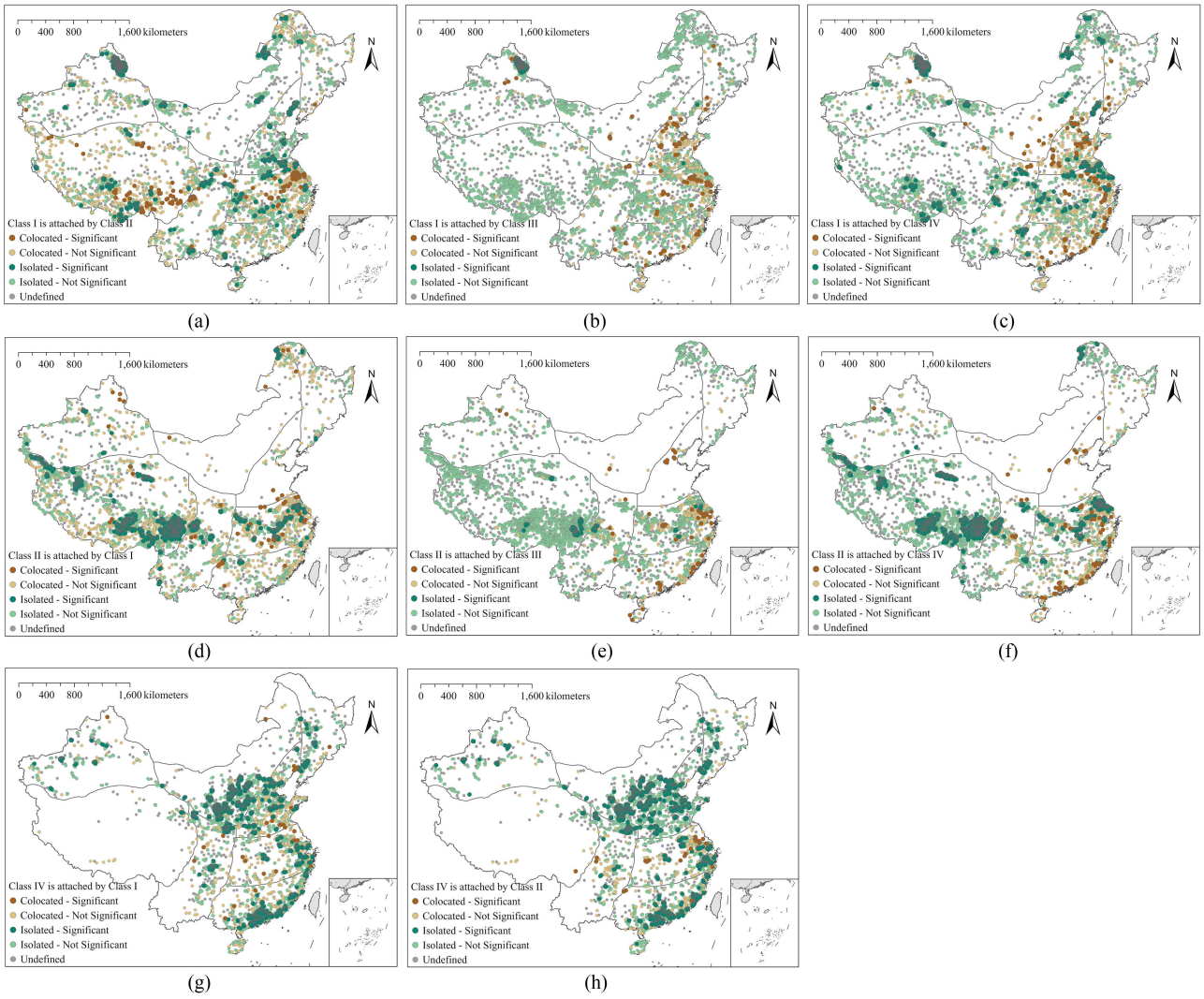

Fig. 8. LCLQ for different anomalous regions. (a)–(c) LCLQ by which Class I is attracted to Class II, Class III, and Class IV, respectively. (d)–(f) LCLQ by which Class II is attracted to Class I, Class III, and Class IV, respectively. (g) and (h) LCLQ through which Class IV is attracted by Class I and Class II, respectively.

E. Driving Forces of Vegetation Change

Although copula functions have been used to model the probability of encountering different vegetation changes under different conditions, the driving forces behind these changes have not been identified. A commonly used tool for attribution analysis, Geodetector software was used to explain the driving forces behind vegetation change. The classification intervals were set to be greater than 10, and the optimal classification method was selected from the equal intervals, natural breaks, and quantile classification methods. Because Geodetector software is limited to measuring the explanatory power of driving factors, spearman's correlation was also used to analyze the relationships between variables, with both methods showing a high degree of consistency [60]. The impacts of all anomalous regions on the driving factors passed the 95% significance test.

Table VI shows the ranking of the influencing factors of NDVI trend changes due to anomalous regions, from greatest to least, including SW_trend, Prep_trend, Elevation, NTL_trend, Gradient, Temp_trend, SPEI_trend, and aspect. The NDVI trend changes were primarily influenced by SW_trend. SW content synchronously affected vegetation growth, with precipitation having a positive impact on NDVI trends in anomalous regions. The NDVI shows varying growing conditions at different altitudes, with an overall upward trend with increasing altitude, albeit with certain limitations [61]. Table VI shows that different classes of anomalous regions have distinct primary drivers, with human activity being the determining factor for Class III. Meanwhile, SW content continues to dominate the NDVI trends for other types. A factor detector was used to examine the anomalous regions across the eight regions to investigate the primary drivers of anomalous regions within distinct regions (Fig. 9).

Fig. 10 illustrates the interactions and impacts among the variables, showing mainly nonlinear enhancement and double-factor-enhanced types in the explanatory power between variables. This suggests that the variables are coupled and enhanced in their influence on NDVI trends. The interactions between SW_trend and the other variables exhibit nonlinear enhancement

TABLE VI
EXPLANATORY POWER OF NDVI_TREND FACTORS

Class		SW_trend	SPEI_trend	Temp_trend	Prep_trend	NTL_trend	Aspect	Elevation	Gradient
Anomalous regions	q value	0.1936***	–0.0143**	–0.0149**	0.0834**	-0.0494**	0.0023**	0.0671**	0.0335**
	p statistics	0.000	0.000	0.000	0.000	0.000	0.001	0.000	0.000
I	q value	0.0973**	–0.0419**	–0.0163**	0.0361**	–0.0931**	0.0059*	–0.0504**	0.0226**
	p statistics	0.000	0.000	0.000	0.000	0.000	0.015	0.000	0.000
II	q value	0.1437**	0.0096**	0.0092**	–0.1079**	–0.1546**	0.0075**	0.0996**	0.0783**
	p statistics	0.000	0.000	0.000	0.000	0.000	0.001	0.000	0.000
III	q value	0.0387**	0.0271	0.0305	–0.0332*	–0.1259**	–0.0167	–0.0452	–0.0275
	p statistics	0.005	0.117	0.235	0.020	0.000	0.504	0.115	0.070
IV	q value	0.2519**	–0.044**	–0.1014**	0.1002**	–0.0205**	–0.0075**	0.1553**	0.0207**
	p statistics	0.000	0.000	0.000	0.000	0.000	0.006	0.000	0.000

*, ** are coefficients different from zero at 5% and 1% significance levels, respectively.

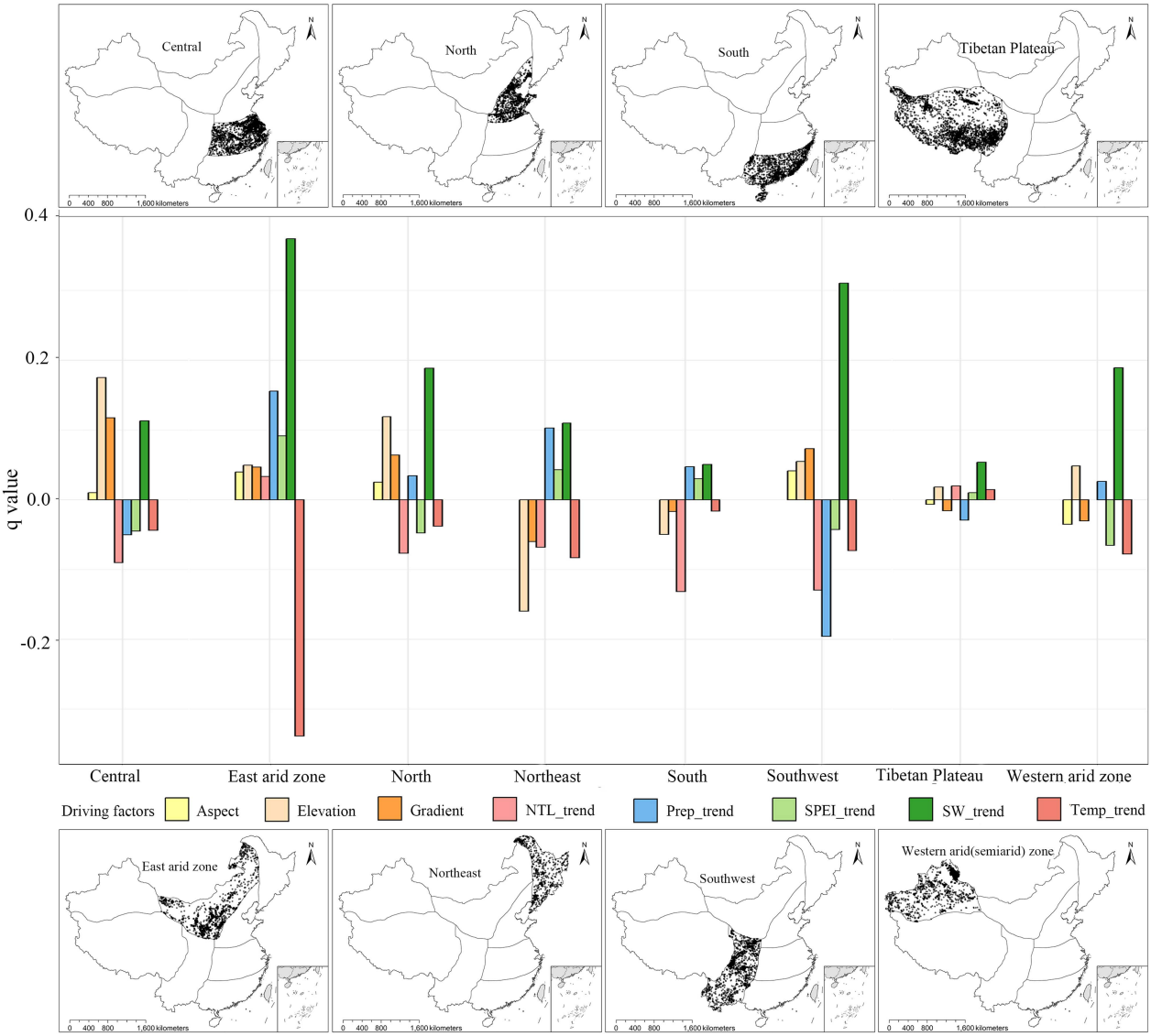

Fig. 9. Significant influences on NDVI_trend in anomalous regions in different regional zones.

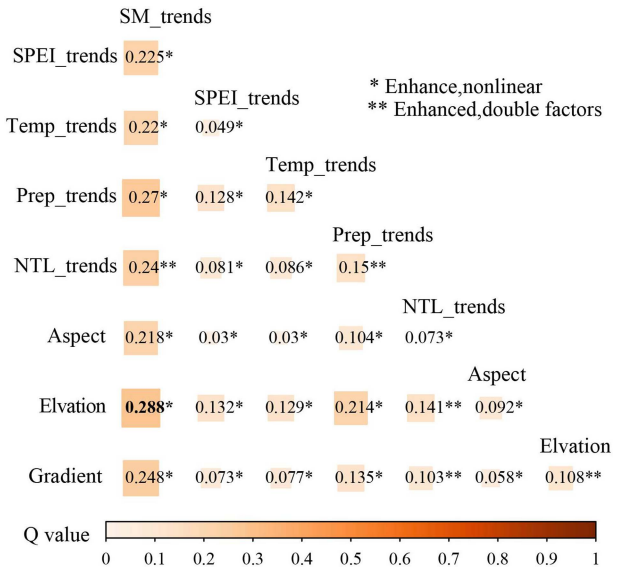

Fig. 10. Interactive detection of factors influencing NDVI_trend. The numerical values represent the explanatory power of the coupled variables for vegetation change.

characteristics with relatively high explanatory power. The most powerful combination, in terms of explanatory strength, was SW_trend and elevation, followed by Prep_trend and SW_trend. This is because precipitation within a certain range tends to increase with increasing elevation, resulting in an increase in SW content, thereby exhibiting a stronger correlation with the NDVI trends. The weakest explanatory power was reflected in the combination of the SPEI_trend and aspect.

IV. Discussion

A. Spatial Correlation Between Vegetation Change and the Environment

To date, a majority of prior studies have focused on examining the contributions and mechanisms of human activity and climate change on vegetation change [15], [62]. They investigated the driving forces behind NDVI changes at both the pixel and overall scales, often without differentiating the anomalous spatial characteristics of the study area. We have used a novel approach by investigating the colocation patterns between NDVI and external anomalous environmental changes in China using the CLQ research method. Given China's extensive land area and considerable geographical diversity, the GCLQ method has failed to capture the complicated connections between vegetation changes and their driving factors. However, research utilizing LCLQ to investigate local changes in anomalous regions in China has revealed significant colocation patterns among regions exhibiting abnormal vegetation changes. These patterns provide insight into the interactions between vegetation distribution and environmental factors. For instance, regions with intense NTL and anomalous temperature or precipitation demonstrate significant dispersion, suggesting that the abnormal vegetation changes in these areas are not solely influenced by climate but are predominantly linked to urban green space development.

B. Climate Influences Vegetation Change

The research findings employing the Copula function indicate that both temperature and precipitation positively influence long-term regional vegetation cover change. Moreover, temperature emerges as the primary climate factor driving these vegetation changes, aligning with prior studies [63]. The regions with anomalous NDVI from temperature and precipitation changes, as defined in this study, were predominantly concentrated in the Tibetan Plateau, western arid (semiarid) zones, and southern China. Despite an increasing precipitation trend, vegetation cover has continued to decrease. This is primarily attributed to increased precipitation promoting vegetation growth as elevation increases in arid mountainous regions. However, increased precipitation also leads to heightened cloud cover and water saturation, intensifying the sensitivity of NDVI to temperature [64]. The correlation between these factors shifted in a positive direction but lacked statistical significance ($p<0.05$). Furthermore, rising temperatures trigger snowmelt [65], which supports regional vegetation greening. Additionally, vegetation growth imposes specific temperature requirements. Exceeding the temperature threshold tolerated by vegetation can lead to detrimental effects on biological enzyme activity, consequently impacting the vegetation's life cycle [54], [66].

C. Impact of Human Activities

Given significant spatial heterogeneity across China, the distinct anomalous regions are influenced by various external factors. Our findings suggest that human activities can stimulate vegetation cover increase. This study used the change in NTL as a proxy for human activities to investigate their impact on NDVI change, given the close link between NTL and urbanization. There was a significant negative correlation between NTL changes in the southwest, central, south, northeast, and anomalous regions of NDVI. Class IV represents regions characterized by both robust economic development and greening vegetation, reflecting the varying stages of urbanization [67]. In the initial phases of urban development, land types, including grasslands and forests, are transformed into impervious surfaces owing to land requirements. As urban economies advance, there is a renewed focus on enhancing living environments, such as urban green spaces, leading to vegetation improvements. Vegetation cover in central urban areas often surpasses that of outer urban areas [68]. However, there are exceptions in highly developed urban agglomeration like the Yangtze River Delta [69]. This reflects the spatial distribution of anomalous regions where NTL and NDVI deteriorate simultaneously. According to the copula conditional probability results, the probability of vegetation enhancement remained high as the NTL increased or decreased. This primarily arises from the concentration of nationwide population changes within urban areas. However, the urban area is small compared to China's total area. Further investigations require the use of more precise data for delineation, particularly to show the occurrence probabilities of vegetation greening and intensity of human activity in distinct regions, particularly within urban domains.

Population migration influences the intensity of land use activities, thereby driving vegetation changes. In regions of China with substantial population increases, NDVI has shown a declining trend, indicating substantial vegetation degradation. Some researchers in China [70] have also highlighted the marginal effects of PD changes on vegetation greening. Here, the changes in NDVI vary with each unit change in the population across different regions. In certain areas of the Tibetan Plateau and the western arid (semiarid) zone, a decrease in population has resulted in a decline in the NDVI. There has been a positive impact of human activities on vegetation cover in these regions [71] Over the last century, rural population growth in the Tibetan region has increased the density of grassland vegetation in densely populated areas through land management and irrigation measures. Extensive land reclamation in Xinjiang has facilitated vegetation restoration [72]. However, owing to the complex surface conditions in these regions, intensive land use has been concentrated in areas with favorable hydrothermal conditions and relatively flat terrain. This study did not capture the significant attraction phenomenon of Class IV in this region, caused by anomalous regions of temperature and precipitation.

D. Policies Affect Vegetation Change

The impact of policies on vegetation has been substantiated [73], [74]. Many afforestation activities and ecological restoration projects implemented over the last century have been beneficial for vegetation restoration. The findings have highlighted the improvement in vegetation in the project area. The Grain for Green Program and Natural Forest Protection Program are key factors contributing to the increase in vegetation in the Loess Plateau and southwest karst areas of China [75], [76]. The Ant Forest Project has expanded the vegetation area of the northwestern desert through shrub planting, effectively combating local soil erosion [77]. As the world's largest afforestation program, the Three-North Shelter Forest Program has substantially enlarged the vegetated area of the project region, effectively preventing and managing land degradation in China [28]. However, ecological restoration projects need to consider local natural conditions and soil environments. In some arid areas, planting trees for ecological restoration can deplete local water resources and exacerbate environmental conditions [78]. This tree-planting approach to vegetation succession also hampered the effectiveness of ecological restoration projects in certain parts of southwest China [79]. To address this, the government has initiated programs such as returning farmland to grassland and rangeland to grassland to restore ecosystems in arid regions [80] Various human activities have diverse feedback effects on vegetation. In this study, regions showing a significant positive correlation with human activities were defined as anomalous regions. The response of vegetation changes in these anomalous regions to human activities has been discussed in detail.

E. Influencing Factors of Vegetation Change Based on Geodetector

According to Geodetector's analysis, SW content is a key factor influencing vegetation change, mainly through its effect on soil moisture on vegetation change. At different depths, the SW content at different depths has a generally similar and positive feedback impact on regional vegetation [43], [81]. In the regions under scrutiny, vegetation generally exhibited a decline, particularly influenced by soil water (SW) content in the southwest, eastern arid, and western arid (semiarid) zones. This trend closely correlates with the water retention capacity of the underlying surfaces [82]. While related studies based on SW content data investigating vegetation responses to extreme climates are relatively common [83], [84], this study did not attention to the time-lagged effect of vegetation in response to drought and cumulative effect. The slope aspect has the lowest influence on regional vegetation. Theoretically speaking, the slope aspect has an impact on the distribution of vegetation in mountainous areas by affecting daylight hours and precipitation patterns [85]. For example, vegetation growth on the shady slope is better than that on the sunny slope in the Tibetan Plateau region. However, the average slope direction in the region is basically unchanged. Thus it is difficult to have a direct impact on the trend of vegetation dynamic. Different vegetation types exhibit varying seasonal responses to precipitation and temperature [86], with shrubs, grasslands, and desert vegetation being more sensitive to climate change [87].

F. Limitations and Directions for Improvement

This study identified regions where the anomalous NDVI distribution was attributed to climate change and human activities. However, it does not separate the specific roles that the climate and human activity have played in influencing the vegetation. This research primarily pays attention to examining the influences of climate and PD changes on vegetation using annual data through copula joint functions. Climate effects on vegetation changes significantly across months, particularly during the growing season [88]. Although copula functions have been employed to evaluate the probability of vegetation states in various diverse external conditions, the spatial distribution of these probabilities remains unexplored. Multiple variables have been integrated using vine copula methods to analyze the probability and spatial arrangement of vegetation changes under varying climatic conditions [89], [90]. Future research should further investigate this aspect to provide a more thorough analysis.

V. Conclusion

This study has primarily focused on the anomalous regions of vegetation change in China related to climate change and human activities. These regions refer to areas where temperature and precipitation exhibit a significant negative correlation with NDVI change and regions where NTL and NDVI display a significant positive correlation. In this article, various analytical tools including TS slope, MK test, correlation analysis, Copula function, CLQ, and Geodetector were employed to assess the spatial-temporal changes in NDVI across China from 2000 to 2020. The research aimed to identify anomalous regions, evaluate probabilities of vegetation browning and greening under diverse climate and population pressures, and explore

synchronous patterns and driving factors of vegetation change in these anomalous regions. The results show that:

1) The NDVI in China fluctuated at a rate of 0.00233 per year. It was observed that the overall vegetation recovery in the study area was good, and 46.52% of the total area exhibited a significant increase in overall vegetation change, which was primarily concentrated in northern China. Conversely, significant vegetation degradation was noted in the Pearl River Delta, Ili River Valley region, Yangtze River Delta, southern Tibetan Plateau, and eastern arid zone. The northeastern region demonstrated the major amounts of areas with a significant increase in vegetation, whereas the eastern arid zone showed a significant decrease.
2) Correlation analysis showed that precipitation and temperature in China generally exhibit a positive correlation with NDVI, and both showed significant spatial heterogeneity. The anomalous regions outlined in this study were primarily concentrated in the Tibetan Plateau and eastern coastal area. The copula conditional probability analysis indicated that temperature had a more pronounced influence on vegetation growth than precipitation. Both factors played supportive roles, whereas PD had an opposing effect. The probability of synchronization of vegetation changes in the Tibetan Plateau, eastern arid zone, and western arid (semiarid) zone was higher.
3) LCLQ analysis was used to identify whether significant localized colocation patterns existed between anomalous regions and to interpret the aggregation results of these regions.
4) Geodetector software was used to investigate the influencing factors of vegetation change in the anomalous regions. This showed that SW content, precipitation, and elevation were the primary determinants. Among these interactions, the nonlinear relationship between SW content and elevation had the strongest impact on vegetation dynamics.

The 2019 IPCC report highlighted the intensification of the global greenhouse effect. Since 1850, the average global temperature has risen by 1.53°C, leading to frequent extreme weather events that significantly impact food production and exacerbate land desertification. Strengthening forest vegetation restoration and enhancing the carbon absorption capacity of terrestrial ecosystems are crucial strategies endorsed by the international community to achieve global "carbon neutrality." China has undertaken extensive global vegetation restoration projects, contributing a quarter of the world's vegetation restoration efforts. It is important, however, to evaluate these projects realistically: they focus on restoring vegetation in areas affected by desertification rather than transforming desert areas. When implementing local afforestation programs, practical considerations such as water and soil resources must be carefully weighed. The findings of our research have considerable value for determining the mechanisms by which vegetation interacts with the external environment. The results have provided key insights for guiding vegetation conservation planning.

REFERENCES

[1] F. Jin, W. Yang, J. Fu, and Z. Li, "Effects of vegetation and climate on the changes of soil erosion in the Loess plateau of China," *Sci. Total Environ.*, vol. 773, Jun. 2021, Art. no. 145514.

[2] Y. Li et al., "Potential and actual impacts of deforestation and afforestation on land surface temperature," *J. Geophys. Res.: Atmospheres*, vol. 121, no. 24, pp. 14,372–14,386, 2016.

[3] Y. Pan et al., "A large and persistent carbon sink in the world's forests," *Science*, vol. 333, no. 6045, pp. 988–993, Aug. 2011.

[4] W. Li, J. Xu, Y. Yao, and Z. Zhang, "Temporal and spatial changes in the vegetation cover (NDVI) in the three-river headwater region, tibetan plateau, China under global warming," *Mountain Res.*, vol. 39, no. 4, pp. 473–482, 2021.

[5] A.P. P. Hartoyo, A. Sunkar, R. Ramadani, S. Faluthi, and S. Hidayati, "Normalized difference vegetation index (NDVI) analysis for vegetation cover in Leuser Ecosystem area, Sumatra, Indonesia," *Biodiversitas J. Biol. Divers.*, vol. 22, no. 3, Feb. 2021, Art. no. 3.

[6] S. A. Shammi and Q. Meng, "Use time series NDVI and EVI to develop dynamic crop growth metrics for yield modeling," *Ecological Indicators*, vol. 121, Feb. 2021, Art. no. 107124.

[7] J. Wang, P. M. Rich, and K. P. Price, "Temporal responses of NDVI to precipitation and temperature in the central Great Plains, USA," *Int. J. Remote Sens.*, vol. 24, no. 11, pp. 2345–2364, Jan. 2003.

[8] H. Wang, Z. Li, L. Cao, R. Feng, and Y. Pan, "Response of NDVI of natural vegetation to climate changes and drought in China," *Land*, vol. 10, no. 9, 2021, Art. no. 966.

[9] M. G. Ghebrezgabher, T. Yang, X. Yang, and T. E. Sereke, "Assessment of NDVI variations in responses to climate change in the Horn of Africa," *Egyptian J. Remote Sens. Space Sci.*, vol. 23, no. 3, pp. 249–261, Dec. 2020.

[10] L. Jiang, Y. Liu, S. Wu, and C. Yang, "Analyzing ecological environment change and associated driving factors in China based on NDVI time series data," *Ecological Indicators*, vol. 129, Oct. 2021, Art. no. 107933.

[11] X. Meng, X. Gao, S. Li, and J. Lei, "Spatial and temporal characteristics of vegetation NDVI changes and the driving forces in Mongolia during 1982–2015," *Remote Sens.*, vol. 12, no. 4, Jan. 2020, Art. no. 603.

[12] H. Yang, J. Hu, S. Zhang, L. Xiong, and Y. Xu, "Climate variations vs. human activities: Distinguishing the relative roles on vegetation dynamics in the three karst provinces of Southwest China," *Front. Earth Sci.*, vol. 10, Apr. 2022, Art. no. 799493.

[13] L. Luo et al., "Research on the correlation between NDVI and climatic factors of different vegetation in the Northeast China," *Acta Botanica Boreali-Occidentalia Sinica*, vol. 29, no. 4, pp. 800–808, 2009.

[14] L. Zhu, J. Meng, and L. Zhu, "Applying Geodetector to disentangle the contributions of natural and anthropogenic factors to NDVI variations in the middle reaches of the Heihe River Basin," *Ecological Indicators*, vol. 117, Oct. 2020, Art. no. 106545.

[15] W. Gao et al., "NDVI-based vegetation dynamics and their responses to climate change and human activities from 1982 to 2020: A case study in the Mu Us Sandy Land, China," *Ecological Indicators*, vol. 137, Apr. 2022, Art. no. 108745.

[16] L. Sun et al., "Impacts of climate change and human activities on NDVI in the Qinghai-Tibet plateau," *Remote Sens*, vol. 15, no. 3, Jan. 2023, Art. no. 587.

[17] J. Zeng, X. Cui, W. Chen, and X. Yao, "Impact of urban expansion on the supply-demand balance of ecosystem services: An analysis of prefecture-level cities in China," *Environ. Impact Assessment Rev.*, vol. 99, Mar. 2023, Art. no. 107003.

[18] X. Liu et al., "Impacts of urban expansion on terrestrial carbon storage in China," *Environ. Sci. Technol.*, vol. 53, no. 12, pp. 6834–6844, Jun. 2019.

[19] Y. Zhang, X. Zhao, J. Gong, F. Luo, and Y. Pan, "Effectiveness and driving mechanism of ecological restoration efforts in China from 2009 to 2019," *Sci. Total Environ.*, vol. 910, Feb. 2024, Art. no. 168676.

[20] T. Chen, Q. Wang, Y. Wang, and L. Peng, "Processes and mechanisms of vegetation ecosystem responding to climate and ecological restoration in China," *Front. Plant Sci.*, vol. 13, Nov. 2022, Art. no. 1062691.

[21] T. Chen, Y. Wang, and L. Peng, "Exploring social-ecological system resilience in South China karst: Quantification, interaction, and policy implication," *Geography Sustainability*, vol. 5, no. 2, pp. 289–301, Jun. 2024.

[22] J. Tan, L. Peng, W. Wu, and Q. Huang, "Mapping the evolution patterns of urbanization, ecosystem service supply–demand, and human well-being: A tree-like landscape perspective," *Ecological Indicators*, vol. 154, Oct. 2023, Art. no. 110591.

[23] P. Vahmani, F. Sun, A. Hall, and G. Ban-Weiss, "Investigating the climate impacts of urbanization and the potential for cool roofs to counter future climate change in Southern California," *Environ. Res. Lett.*, vol. 11, no. 12, Dec. 2016, Art. no. 124027.
[24] K. Huang, L. Peng, X. Wang, W. Deng, and Y. Liu, "Incorporating circuit theory, complex networks, and carbon offsets into the multi-objective optimization of ecological networks: A case study on karst regions in China," *J. Cleaner Prod.*, vol. 383, Jan. 2023, Art. no. 135512.
[25] J. Huang et al., "Climate change and ecological engineering jointly induced vegetation greening in global karst regions from 2001 to 2020," *Plant Soil*, vol. 475, no. 1, pp. 193–212, Jun. 2022.
[26] T. Chen, Y. Wang, and L. Peng, "Advanced time-lagged effects of drought on global vegetation growth and its social risk in the 21st century," *J Environ. Manage.*, vol. 347, Dec. 2023, Art. no. 119253.
[27] J.-H. Jeong et al., "Greening in the circumpolar high-latitude may amplify warming in the growing season," *Climate Dyn.*, vol. 38, no. 7, pp. 1421–1431, Apr. 2012.
[28] B. Qiu, G. Chen, Z. Tang, D. Lu, Z. Wang, and C. Chen, "Assessing the Three-North Shelter Forest Program in China by a novel framework for characterizing vegetation changes," *ISPRS J. Photogrammetry Remote Sens.*, vol. 133, pp. 75–88, Nov. 2017.
[29] L. Li et al., "Spatiotemporal patterns of vegetation greenness change and associated climatic and anthropogenic drivers on the Tibetan plateau during 2000–2015," *Remote Sens.*, vol. 10, no. 10, Oct. 2018, Art. no. 1525.
[30] S. Piao et al., "Interannual variations of monthly and seasonal normalized difference vegetation index (NDVI) in China from 1982 to 1999," *J. Geophys. Res. Atmospheres*, vol. 108, no. D14, pp. 1160–1171, 2003.
[31] L. Yuan et al., "The influence of oil exploitation on the degradation of vegetation: A case study in the Yellow River Delta Nature Reserve, China," *Environ. Technol. Innov.*, vol. 28, Nov. 2022, Art. no. 102579.
[32] W. Zhou et al., "Dynamic of grassland vegetation degradation and its quantitative assessment in the northwest China," *Acta Oecologica*, vol. 55, pp. 86–96, Feb. 2014.
[33] X. Fan, P. Gao, B. Tian, C. Wu, and X. Mu, "Spatio-temporal patterns of NDVI and its influencing factors based on the ESTARFM in the Loess plateau of China," *Remote Sens.*, vol. 15, no. 10, Jan. 2023, Art. no. 2553.
[34] P. S. A. Beck, C. Atzberger, K. A. Høgda, B. Johansen, and A. K. Skidmore, "Improved monitoring of vegetation dynamics at very high latitudes: A new method using MODIS NDVI," *Remote Sens. Environ.*, vol. 100, no. 3, pp. 321–334, Feb. 2006.
[35] J. Zhang and L. Zhiguang, *Climate of China*. Shanghai, China: Shanghai Scientific and Technical Publishers, 1985.
[36] M. Xiao, Q. Zhang, V. P. Singh, and X. Chen, "Regionalization-based spatiotemporal variations of precipitation regimes across China," *Theor. Appl. Climatol.*, vol. 114, no. 1, pp. 203–212, Oct. 2013.
[37] J. Gao et al., "China regional 250 m normalized difference vegetation index data set (2000–2023)," *Natl. Tibet. Plateau Third Pole Environ. Data Cent.*, 2022, doi: 10.11888/Terre.tpdc.300330.
[38] Z. Chen et al., " An extended time series (20002018) of global NPP-VIIRS-like nighttime light data from a cross-sensor calibration," *Earth Syst. Sci. Data*, vol. 13, pp. 889–906, May 3, 2021, doi: 10.5194/essd-13-889-2021.
[39] S. Peng, "1 km monthly temperature and precipitation dataset for China from 1901 to 2022," *Earth System Sci. Data*, 2021, doi: 10.12041/geodata.164304785536614.ver1.db.
[40] S. Peng, Y. Ding, Z. Wen, Y. Chen, Y. Cao, and J. Ren, "1 km monthly potential evapotranspiration dataset for China from 1901 to 2022," *Earth System Sci. Data*, 2022, doi: 10.11866/db.loess.2021.001.
[41] C. Zheng, L. Jia, and T. Zhao, "Global daily surface soil moisture dataset at 1-km resolution (2000–2020)," *Natl. Tibet. Plateau Third Po-le Environ. Data Cent.*, 2022, doi: 10.1038/s41597-023-01991-w.
[42] Y. Xu et al., "Identification of ecologically sensitive zones affected by climate change and anthropogenic activities in Southwest China through a NDVI-based spatial-temporal model," *Ecological Indicators*, vol. 158, Jan. 2024, Art. no. 111482.
[43] W. Jiang, L. Yuan, W. Wang, R. Cao, Y. Zhang, and W. Shen, "Spatio-temporal analysis of vegetation variation in the Yellow River Basin," *Ecological Indicators*, vol. 51, pp. 117–126, Apr. 2015.
[44] B. Hussain, N. A. Qureshi, R. A. Buriro, S. S. Qureshi, A. A. Pirzado, and T. A. Saleh, "Interdependence between temperature and precipitation: Modeling using copula method toward climate protection," *Model. Earth Syst. Environ.*, vol. 8, no. 2, pp. 2753–2766, Jun. 2022.
[45] B.-C. Jhong and C.-P. Tung, "Evaluating future joint probability of precipitation extremes with a copula-based assessing approach in climate change," *Water Resour. Manage.*, vol. 32, no. 13, pp. 4253–4274, Oct. 2018.
[46] G. Lazoglou and C. Anagnostopoulou, "Joint distribution of temperature and precipitation in the Mediterranean, using the Copula method," *Theor. Appl. Climatol.*, vol. 135, no. 3, pp. 1399–1411, Feb. 2019.
[47] T. F. Leslie and B. J. Kronenfeld, "The colocation quotient: A New measure of spatial association between categorical subsets of points," *Geographical Anal.*, vol. 43, no. 3, pp. 306–326, 2011.
[48] R. G. Cromley, D. M. Hanink, and G. C. Bentley, "Geographically weighted colocation quotients: Specification and application," *Professional Geographer*, vol. 66, no. 1, pp. 138–148, Jan. 2014.
[49] J. Wang and C. Xu, "Geodetector: Principle and prospective," *Acta Geographica Sinica*, vol. 72, no. 1, pp. 116–134, 2017.
[50] N. A. Rybnikova and B. A. Portnov, "Mapping geographical concentrations of economic activities in Europe using light at night (LAN) satellite data," *Int. J. Remote Sens.*, vol. 35, no. 22, pp. 7706–7725, Nov. 2014.
[51] C. Li, G. Chen, J. Luo, S. Li, and J. Ye, "Port economics comprehensive scores for major cities in the Yangtze Valley, China using the DMSP-OLS night-time light imagery," in *Remote Sensing of Night-Time Light*. London, U.K.: Routledge, 2021, pp. 147–170.
[52] H. Ci and Q. Zhang, "Spatio-temporal patterns of NDVI variations and possible relations with climate changes in xinjiang province," *J. Geo-Inf. Sci.*, vol. 19, no. 5, pp. 662–671, 2017.
[53] J. Busch and O. Amarjargal, "100 global bright spots of green growth: Co-occurrence of nighttime light gain and forest gain, 1990–2015," *Glob. Environ. Change*, vol. 75, Jul. 2022, Art. no. 102556.
[54] Y. Cui et al., "Estimating and analyzing the optimum temperature for vegetation growth in China," *J. Natural Resour.*, vol. 27, no. 2, pp. 281–292, Feb. 2012.
[55] Y. Hu, H. J. Miller, and X. Li, "Detecting and analyzing mobility hotspots using surface networks," *Trans. GIS*, vol. 18, no. 6, pp. 911–935, 2014.
[56] M. Gottfried et al., "Continent-wide response of mountain vegetation to climate change," *Nature Climate Change*, vol. 2, no. 2, pp. 111–115, Feb. 2012.
[57] H. Sun et al., "Analysis of the vegetation cover change and the relationship btween NDVI and environmental factors by using NOAA time series data," *Nat. Remote Sens. Bull.*, vol. 3, pp. 204–210, 2021.
[58] S. Zhao, S. Liu, and D. Zhou, "Prevalent vegetation growth enhancement in urban environment," *Proc. Nat. Acad. Sci.*, vol. 113, no. 22, pp. 6313–6318, 2016.
[59] J. Zhang, Q. Zhang, L. Yang, and D. Li, "Seasonal characters of regional vegetation activity in response to climate change in West China in recent 20 years," *J. Geographical Sci.*, vol. 16, no. 1, pp. 78–86, Jan. 2006.
[60] T. Yang, F. Sun, W. Liu, H. Wang, T. Wang, and C. Liu, "Using geo-detector to attribute spatio-temporal variation of pan evaporation across China in 1961–2001," *Int. J. Climatol.*, vol. 39, no. 5, pp. 2833–2840, 2019.
[61] D. Xu, K. Zhang, L. Cao, X. Guan, and H. Zhang, "Driving forces and prediction of urban land use change based on the Geodetector and CA-Markov model: A case study of Zhengzhou, China," *Int. J. Digit. Earth*, vol. 15, no. 1, pp. 2246–2267, Dec. 2022.
[62] H. Chu, S. Venevsky, C. Wu, and M. Wang, "NDVI-based vegetation dynamics and its response to climate changes at Amur-Heilongjiang river basin from 1982 to 2015," *Sci. Total Environ.*, vol. 650, pp. 2051–2062, Feb. 2019.
[63] M. Meng, J. Ni, and M. Zong, "Impacts of changes in climate variability on regional vegetation in China: NDVI-based analysis from 1982 to 2000," *Ecol. Res.*, vol. 26, no. 2, pp. 421–428, Mar. 2011.
[64] R. P. Bartholomeus, J.-P. M. Witte, P. M. van Bodegom, J. C. van Dam, P. de Becker, and R. Aerts, "Process-based proxy of oxygen stress surpasses indirect ones in predicting vegetation characteristics," *Ecohydrology*, vol. 5, no. 6, pp. 746–758, 2012.
[65] W. Ta, Z. Dong, and C. Sanzhi, "Effect of the 1950s large-scale migration for land reclamation on spring dust storms in Northwest China," *Atmos. Environ.*, vol. 40, no. 30, pp. 5815–5823, Sep. 2006.
[66] F. S. Chapin, "Direct and indirect effects of temperature on arctic plants," *Polar Biol.*, vol. 2, no. 1, pp. 47–52, Jun. 1983.
[67] W. Fu, Y. Lü, P. Harris, A. Comber, and L. Wu, "Peri-urbanization may vary with vegetation restoration: A large scale regional analysis," *Urban Forestry Urban Greening*, vol. 29, pp. 77–87, Jan. 2018.
[68] R. Yao, L. Wang, X. Huang, X. Chen, and Z. Liu, "Increased spatial heterogeneity in vegetation greenness due to vegetation greening in mainland China," *Ecological Indicators*, vol. 99, pp. 240–250, Apr. 2019.
[69] D. Li, S. Wu, Z. Liang, and S. Li, "The impacts of urbanization and climate change on urban vegetation dynamics in China," *Urban Forestry Urban Greening*, vol. 54, Oct. 2020, Art. no. 126764.

[70] W. Li, X. Li, M. Tan, and Y. Wang, "Influences of population pressure change on vegetation greenness in China's mountainous areas," *Ecol. Evol.*, vol. 7, no. 21, pp. 9041–9053, 2017.
[71] H. Ganjurjav et al., "Alpine grassland ecosystem respiration variation under irrigation in Northern Tibet," *Acta Ecologica Sinica*, vol. 34, no. 5, pp. 271–276, 2014.
[72] J. Wang, K. L. Wang, M. Y. Zhang, and Y. F. Duan, "Temporal-spatial variation in NDVI and drivers in hilly terrain of Southern China," *Resour. Sci.*, vol. 36, no. 8, pp. 1712–1723, 2014.
[73] W. Song, Y. Feng, and Z. Wang, "Ecological restoration programs dominate vegetation greening in China," *Sci. Total Environ.*, vol. 848, Nov. 2022, Art. no. 157729.
[74] X. Fan, Y. Qu, J. Zhang, and E. Bai, "China's vegetation restoration programs accelerated vegetation greening on the loess plateau," *Agricultural Forest Meteorol.*, vol. 350, May 2024, Art. no. 109994.
[75] S. Li et al., "Vegetation changes in recent large-scale ecological restoration projects and subsequent impact on water resources in China's loess plateau," *Sci. Total Environ.*, vol. 569–570, pp. 1032–1039, Nov. 2016.
[76] Y. Qiao, Y. Jiang, and C. Zhang, "Contribution of karst ecological restoration engineering to vegetation greening in southwest China during recent decade," *Ecological Indicators*, vol. 121, Feb. 2021, Art. no. 107081.
[77] Y. Cai et al., "Vegetation cover changes in China induced by ecological restoration-protection projects and land-use changes from 2000 to 2020," *CATENA*, vol. 217, Oct. 2022, Art. no. 106530.
[78] L. Huang et al., "Effects of grassland restoration programs on ecosystems in arid and semiarid China," *J. Environ. Manage.*, vol. 117, pp. 268–275, Mar. 2013.
[79] X. Tong et al., "Quantifying the effectiveness of ecological restoration projects on long-term vegetation dynamics in the karst regions of Southwest China," *Int. J. Appl. Earth Observ. Geoinf.*, vol. 54, pp. 105–113, Feb. 2017.
[80] S. Cao, "Why large-scale afforestation efforts in China have failed to solve the desertification problem," *Environ. Sci. Technol.*, vol. 42, no. 6, pp. 1826–1831, May 2008.
[81] Y. Guan et al., "Vegetation response to climate zone dynamics and its impacts on surface soil water content and albedo in China," *Sci. Total Environ.*, vol. 747, Dec. 2020, Art. no. 141537.
[82] D. Penna, M. Borga, D. Norbiato, and G. D. Fontana, "Hillslope scale soil moisture variability in a steep alpine terrain," *J. Hydrol.*, vol. 364, no. 3, pp. 311–327, Jan. 2009.
[83] W. Li, Y. Wang, J. Yang, and Y. Deng, "Time-lag effect of vegetation response to volumetric soil water content: A case study of Guangdong Province, Southern China," *Remote Sens.*, vol. 14, no. 6, Jan. 2022, Art. no. 1301.
[84] L. Chen, Z. Huang, J. Gong, B. Fu, and Y. Huang, "The effect of land cover/vegetation on soil water dynamic in the hilly area of the loess plateau, China," *CATENA*, vol. 70, no. 2, pp. 200–208, Jul. 2007.
[85] G. Yin et al., "Polar-facing slopes showed stronger greening trend than equatorial-facing slopes in Tibetan plateau grasslands," *Agricultural Forest Meteorol.*, vol. 341, Oct. 2023, Art. no. 109698.
[86] G. Zhang, X. Xu, C. Zhou, H. Zhang, and H. Ouyang, "Responses of grassland vegetation to climatic variations on different temporal scales in Hulun Buir grassland in the past 30 years," *J. Geographical Sci.*, vol. 21, no. 4, pp. 634–650, Aug. 2011.
[87] X. W. Chuai, X. J. Huang, W. J. Wang, and G. Bao, "NDVI, temperature and precipitation changes and their relationships with different vegetation types during 1998–2007 in Inner Mongolia, China," *Int. J. Climatol.*, vol. 33, no. 7, pp. 1696–1706, 2013.
[88] Z. Liu, C. Li, P. Zhou, and X. Chen, "A probabilistic assessment of the likelihood of vegetation drought under varying climate conditions across China," *Sci. Rep.*, vol. 6, no. 1, Oct. 2016, Art. no. 35105.
[89] H. W. Li, Y. P. Li, G. H. Huang, and J. Sun, "Quantifying effects of compound dry-hot extremes on vegetation in Xinjiang (China) using a vine-copula conditional probability model," *Agricultural Forest Meteorol.*, vol. 311, Dec. 2021, Art. no. 108658.
[90] G. Zhang et al., "Evaluating vegetation vulnerability under compound dry and hot conditions using vine copula across global lands," *J. Hydrol.*, vol. 631, Mar. 2024, Art. no. 130775.

Xinyue Zhang received the bachelor's degree in geographic information science in 2023 from Sichuan Normal University, Chengdu, China, where she is currently working toward the postgraduate degree majoring in cartography and geographic information systems.

Her study area is the optimization spatial pattern of land use.

Li Peng received the Ph.D. degree in physical geography from the Institute of Mountain Hazards and Environment, Chinese Academy of Sciences, Chengdu, China, in 2013.

Since 2019, he has been a Professor with Sichuan Normal University, Chengdu, China. He has wide experience in the field of mountain area study publishing more than 80 papers in peer-reviewed journals such as *Land Degradation and Development*, *Remote Sensing*, *Journal of Cleaner Production*, *Environmental Research Letter*, and *International Journal of Disaster Risk Reduction*. Meanwhile, he serves as a Reviewer of more than 20 international peer-reviewed journals. His research interests include mountain hazards monitoring, remote sensing and GIS technologies for sustainable ecosystem management, and remote sensing data analysis for mountain development.

Jing Tan received the bachelor's degree in human geography from Neijiang Normal University, Neijiang, China, in 2022. She is currently working toward the postgraduate degree majoring in human geography with Sichuan Normal University, Chengdu, China.

Her study area is social-ecological system services.

Huijuan Zhang received the bachelor's degree in international economics and trade from Zhejiang Yuexiu University of Foreign Languages, Shaoxing, China, in 2023. She is currently working toward the postgraduate degree majoring in human geography with Sichuan Normal University, Chengdu, China.

Her research interests include environmental perception, livelihood, and well-being.

Huan Yu received the Ph.D. degree in physical geography from the Northeast Institute of Geography and Agroecology, Chinese Academy of Sciences, Chengdu, China, in 2010.

He is currently a Professor with the Chengdu University of Technology, Chengdu. He has authored or coauthored more than 100 papers in related journals including *Critical Reviews in Environmental Science and Technology*, *Geoderma*, and *Journal of Hydrology*. His research interests include remote sensing and GIS technologies for ecological environments.